Renewable Energy 163 (2021) 78–87

Contents lists available at ScienceDirect

Renewable Energy

journal homepage: www.elsevier.com/locate/renene

Analysis of a biogas-fed SOFC CHP system based on multi-scale hierarchical modeling

Yuqing Wang [a, b, **], Lukas Wehrle [b], Aayan Banerjee [c, d], Yixiang Shi [e], Olaf Deutschmann [b, *]

[a] National Key Laboratory on Electromechanical Dynamic Control, Beijing Institute of Technology, Beijing, 100081, China
[b] Institute for Chemical Technology and Polymer Chemistry, Karlsruhe Institute of Technology, 76133, Karlsruhe, Germany
[c] Department of Earth Science and Engineering, Imperial College London, SW7 2BP, London, UK
[d] Catalytic Processes and Materials Group, Faculty of Science and Technology, MESA+ Institute for Nanotechnology, University of Twente, PO Box 217, 7500, AE Enschede, the Netherlands
[e] Key Laboratory for Thermal Science and Power Engineering of Ministry of Education, Department of Energy and Power Engineering, Tsinghua University, Beijing, 100084, China

ARTICLE INFO

Article history:
Received 17 January 2020
Received in revised form
10 July 2020
Accepted 19 August 2020
Available online 20 August 2020

Keywords:
Biogas
Solid oxide fuel cell
Combined heat and power system
Hierarchical model

ABSTRACT

Biogas is an abundant renewable energy source which can be produced by anaerobic treatment of biological waste such as sewage sludge, agro-industrial waste, and industrial animal waste. The utilization of biogas instead of fossil fuels in a solid oxide fuel cell (SOFC)-based system is a promising choice to achieve a fossil-free and sustainable energy future. A biogas-fed decentralized SOFC combined heat and power (CHP) system model is proposed and analyzed. The system consists of a pre-reformer, an SOFC stack, an afterburner and a heat-recovery boiler. The system model integrates a multi-scale hierarchical three-dimensional SOFC stack model with zero-dimensional balance of power component models, which enables simultaneous investigations of both the overall system performance and the stack-internal distributed properties down to the electrode scale. The effects of steam/carbon ratio, biogas composition and operation voltage of the SOFC stack on the electrical and CHP efficiencies of the system, as well as the temperature gradient within the SOFC stack were studied. The proposed system model is demonstrated as an insightful and powerful tool for designing hybrid SOFC combined heat and power systems.

1. Introduction

Biogas is an abundant renewable energy source which can convert waste into energy. It is typically produced by anaerobic treatment of biological waste such as sewage sludge, agro-industrial waste, and industrial animal waste [1]. The produced biogas mainly consists of 50–70 vol% CH_4 and 30–50 vol% CO_2. The utilization of biogas has attracted great attention since it can help reduce both the emission of greenhouse gases and the consumption of fossil fuels. Biogas energy is regarded to be suitable for small and medium-scale distributed power generation due to large available quantities and wide distribution [2].

Power turbines and internal combustion engines are typically used to convert the biogas energy to produce heat and power at small and medium scales. Compared to the conventional prime movers, fuel cells are advantageous due to their high efficiency, low noise and low pollutant emissions. Among various kinds of fuel cells, the solid oxide fuel cell (SOFC) operates at a relatively high temperature (typically 700–1000 °C) and is most attractive for the combined heat and power (CHP) application based on biogas [3]. In an SOFC-based CHP system, the high-temperature heat of the SOFC is usually recovered by a boiler for heating water and/or an absorption chiller for cooling. More recently, alternative methods have also been considered for recovering the waste heat, such as the vacuum thermionic generator [4] and the cascading thermoelectric generator and cooler [5], next to more.

The feasibility of using biogas in the SOFC has been experimentally investigated in lab-scale single cell, stack and even in

* Corresponding author.
** Corresponding author. National Key Laboratory on Electromechanical Dynamic Control, Beijing Institute of Technology, Beijing, 100081, China.
E-mail addresses: wangyq@bit.edu.cn (Y. Wang), deutschmann@kit.edu (O. Deutschmann).

https://doi.org/10.1016/j.renene.2020.08.091
0960-1481/

system level [6]. On the single cell level, the research is mainly focused on the feasibility of direct internal reforming of biogas in the SOFC [7,8], the effect of impurities on the anode catalytic activity [9–12], as well as the development of novel anode materials for biogas feeding [13,14]. Further, some trials have been made on developing and testing biogas-fed SOFC prototype systems [15,16]. The DEMOSOFC EU project funded by the Fuel Cell & Hydrogen Joint Undertaking (FCH2-JU) aimed for the installation of the largest biogas-fed SOFC plant in Europe with a power output of 174 kW. The plant has been operated for more than 7000 h since the end of 2017 [17].

Although the potential of developing SOFC-based CHP system fueled with biogas has drawn attention recently, the physical and chemical properties of biogas pose certain challenges to the commercialization of the biogas-fed SOFC CHP system [2]. Biogas contains a large portion of CO_2 and a lower amount of methane than natural gas, which could reduce the useful fuels provided to the SOFC anode and further limit the SOFC performance. Besides, biogas has a low calorific value, which requires a much higher inlet flow rate than would be needed for running on pure methane, to reach an equivalent stack power density. This calls for a careful design of stack and BOP operation parameters so that the system units can be coupled in an optimal way to each other. Moreover, the composition of the biogas is quite fluctuating depending on the properties of the feedstock and the production processes. The varying biogas composition will lead to composition changes of the SOFC anode feed gases so that the CHP system may have to operate far from the design point.

In order to deal with the challenges listed above, the performance of biogas-fed SOFC systems has been extensively evaluated by using computer simulations [18]. Although the high operating temperature enables the direct utilization of biogas in SOFCs, it may lead to carbon deposition along/across the anode and further decrease the SOFC performance. Some novel material design strategies such as alloying with noble metals, using ceria and other oxygen storage materials, etc. [19,20], as well as some alternative structure designs, such as the all porous SOFC [21] have been proposed to resist carbon deposition. For traditional Ni-based anode with conventional designs, an external reforming process is typically applied in the biogas-fed SOFC system to prevent carbon deposition over the anode and increase the SOFC performance [22]. Several system simulations focused on the investigation of various reforming options in the biogas-fed SOFC plant [23]. Farhad et al. studied the effects of fuel processing methods on industrial scale biogas-fueled SOFC system [24]. The results showed that the anode gas recirculation and steam reforming fuel processor-based systems are suitable to be applied for the CHP generation in wastewater treatment plants (WWTPs). Manenti et al. developed a model of an integrated tri-reformer/SOFC system in which the tri-reforming process consists of a combination of dry reforming, steam reforming and partial oxidation [25]. In addition to steady-state system analysis, D'Andrea et al. developed a dynamic model of a biogas-fed poly-generation system based SOFCs and proposed a robust control system to avoid the damage of the stack under unconventional operation conditions [26]. Moreover, the integration of a gas turbine in the biogas-fed SOFC systems has drawn the researchers' attentions recently. Wongchanapai et al. evaluated the combination of direct-biogas SOFC with micro gas turbine (MGT) in a CHP system and examined the effects of operation conditions on system performance [27]. Ding et al. analyzed the coupling effect of operating parameters on the performance of biogas-fed SOFC-GT hybrid system [28]. Aside from the thermodynamic assessment [29], some techno-economic analysis has also been conducted for the biogas-fed SOFC systems [30]. Shariatzadeh et al. carried out a modeling study on a tri-generation biogas-fed system integrating the SOFC with a chiller and a boiler to analyze the economic performance of using biogas instead of natural gas [31]. Giarola et al. compared the cost and energy performance of a SOFC-based CHP system in WWTPs with conventional alternatives and concluded that SOFCs may become cost competitive in thermally-optimized WWTPs [32]. MosayebNezhad et al. found that the integration of SOFC and MGT in WWTPs offered 12% lower electricity cost compared to the standalone SOFC system [33]. Trendewicz and Braun compared the performance and life cycle costs of biogas-fed SOFC CHP systems ranging from 300 kWe to 6 MWe [34]. The results showed that SOFCs for biogas applications are competitive with other cogeneration technologies.

Although numerous studies have been conducted for the analysis of biogas-fed SOFC systems, typically 0-D or 1-D SOFC models are considered in system-level models without accounting for the detailed parameter distributions in the SOFC stacks. In this study, a biogas-fed SOFC CHP system model was developed by integrating a hierarchical 3-D SOFC stack model with 0-D balance of power (BOP) component models. The hierarchical stack model considers the detailed chemical reactions at Ni surface, the electrochemical reactions at the electrode/electrolyte interface, the 1D+1D mass and momentum conservation along the cell thickness and the gas flow channel, and the 3-D heat transfer at the stack level. Compared with other system models developed in previous literatures, the model enables the simultaneous analysis of the overall system performance and the stack-internal distributed properties down to the electrode scale. The effects of the steam/carbon (S/C) ratio, the biogas composition and the SOFC operation voltage on the system and stack performance were analyzed.

2. System description

2.1. System configuration and implementation

The configuration of the proposed biogas-fed SOFC CHP system model is shown in Fig. 1(a). The system principally consists of a pre-reformer, an SOFC stack, a post-burner and a boiler. The inlet biogas is assumed to be purified by clean up processes during which sulfur and other contaminants are fully removed and the purification processes are not considered in the current study. Purified biogas is provided by a tank and preheated by the hot exhaust from the post-burner before mixing with the steam produced by the evaporator. Then the mixture flows into the pre-reformer in which a large portion of methane is converted to hydrogen and carbon monoxide which are then used as fuel for the SOFC stack. Ambient air is compressed by an air blower and preheated by the hot exhaust before entering the SOFC cathode. Within the stack, the fuel and oxygen from the ambient air is electrochemically converted, producing electricity. The anode exhaust from the SOFC stack, which contains unreacted CH_4, CO and H_2, is further totally oxidized in the post-burner. The hot exhaust from the post-burner is used to provide heat for the pre-reformer, the heat exchanger preheating the biogas, the evaporator, as well as the heat exchanger preheating the air subsequently. Finally, the burner exhaust enters the boiler to produce hot water. The effects of the biogas blower and water pump on the system efficiency are assumed to be negligible in the current study [24].

The system model is implemented in gPROMS ModelBuilder as shown in Fig. 1(b). It consists of a 3-D SOFC stack model and 0-D BOP component models. The BOP components, including a pre-reformer, an air blower, an afterburner, several pipes and heat exchangers are modeled in gPROMS. The simulation code containing the hierarchical SOFC stack model is part of the DETCHEM software package [35]. The communication between the system model and the stack model is implemented via Matlab, which enables the I/O

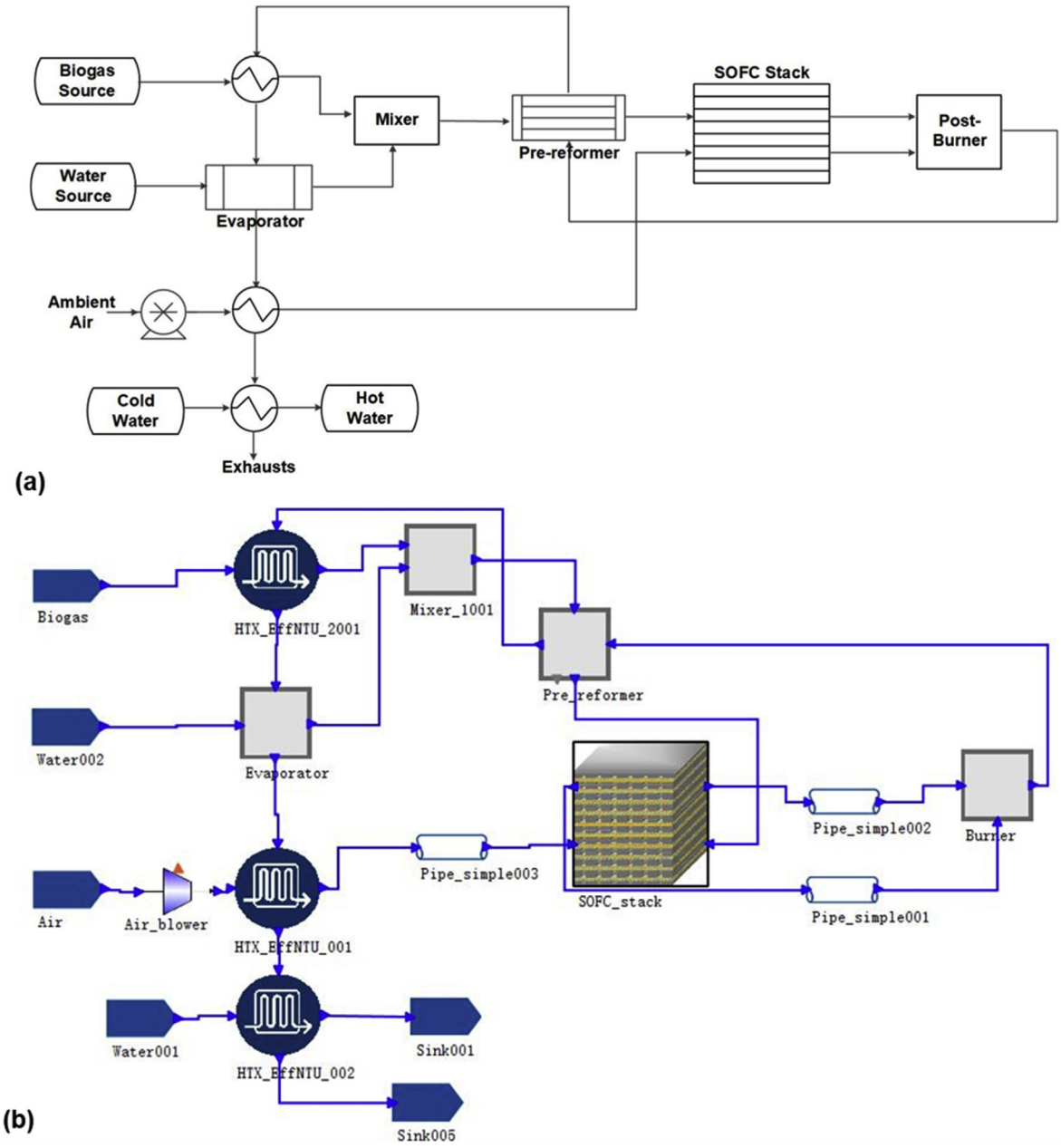

Fig. 1. The biogas-fed SOFC CHP system (a) overall configuration (b) implementation in gPROMS.

(input/output) data transportation between gPROMS and DETCHEM.

2.2. SOFC model

A previously developed hierarchical 3-D SOFC stack model was integrated into the system [36]. The model considers the electrochemical reactions which are assumed to occur at an infinitesimal area around the electrode-electrolyte interface, the thermal reactions within the anode phase at the Ni surface, along with the 1D + 1D thermo-fluidic transport along the thickness and flow direction in a single repeating unit and the 3-D thermal transport across commercial-scale stacks. The mass/charge/momentum/heat transport processes are modeled via a system of differential algebraic equations, as described in detail in Ref. [37]. Since the time scale of the thermal transport in the solid stack is much larger than that of other physical processes, the 3-D thermal transport equation of the solid can be taken out and decoupled from the equation system. A cluster algorithm was then applied to couple the solid phase heat transport equation of the stack and the rest of the equations describing thermo-fluidic and charge transport across individual repeating units by assuming the performance of a repeating unit to be representative of the cluster having a similar local temperature field [36]. The electrochemical reactions are modeled via modified Bulter-Volmer equations considering the parallel pathways of electrochemical oxidation of both H_2 and CO. The thermal reactions which take place in the anode are described by a 42-step reaction mechanism [38]. The applied model and the computation procedure were described in detail in our previous publication [37] and thus not repeated here.

The kinetic model was calibrated with *i*-V curves of an anode-supported single cell (Ni/YSZ-YSZ-LSM /YSZ) measured by

Ebbesen et al. [39] at operating temperatures of 1023.15 K and 1123.15 K with various fuel mixtures (H_2/CO/CO_2/H_2O/Ar) in our previous paper [40]. The calibrated kinetic model was then used in stack simulations. The system is considered to consist of multiple SOFC stacks. Each kW-class stack itself is supposed to consist of 50 anode-supported planer cells, where the cell dimensions are set according to the F-type design of the Forschungzentrum Jülich [41]. The reader is asked to refer to the previous publications of the authors for the detailed geometries and material properties used in the stack simulation [40,42].

2.3. Balance of plant component models

2.3.1. Pre-reformer

The pre-reformer was modeled by considering the thermodynamic equilibriums of the steam reforming (SR) reaction and the water gas shift (WGS) reaction [43]:

$$CH_4 + H_2O \leftrightarrow CO + 3H_2 \tag{1}$$

$$CO + H_2O \leftrightarrow CO_2 + H_2 \tag{2}$$

At thermodynamic equilibrium, the mole fractions of the species can be associated with the equilibrium constant,

$$K_{eq,SR} x_{CH_4} x_{H_2O} = \left(\frac{p}{p_0}\right)^2 x_{CO} x_{H_2}^3 \tag{3}$$

$$K_{eq,WGS} x_{CO} x_{H_2O} = x_{CO_2} x_{H_2} \tag{4}$$

where $K_{eq,SR}$ and $K_{eq,WGS}$ are the equilibrium constant of the SR and WGS reactions respectively, p is the operation pressure, p_0 is the ambient pressure, and x is the mole fraction. The outlet gas composition (H_2, H_2O,C O, CO_2, CH_4, N_2) of the pre-reformer is calculated by combining the conservation of elements C, H, O, N with equations (3) and (4).

The heat required by the pre-reformer is provided by the hot exhaust from the post-burner. The energy balance of the pre-reformer is then calculated by

$$\dot{m}_{in} \sum_i y_{i,in} h_{i,in} + Q = \dot{m}_{in} \sum_i y_{i,out} h_{i,out} \tag{5}$$

$$\dot{m}_H (h_{H,in} - h_{H,out}) = Q \tag{6}$$

where $\dot{m}_{in}$ is the inlet mass flow rate of the biogas-steam mixture, y is the mass fraction of the species, h is the specific enthalpy, $\dot{m}_H$ is the mass flow rate of the hot exhaust, Q is the heat provided by the hot exhaust.

The S/C ratio is a critical parameter of the pre-reformer, which is defined as the ratio of the steam molar flow rate to the molar flow rate of carbon in the biogas fuel,

$$S \Big/ C = \frac{\dot{n}_{H_2O}}{\dot{n}_{CH_4} + \dot{n}_{CO_2}} \tag{7}$$

Sufficient steam should be supplied to the pre-reformer to avoid carbon deposition on the nickel catalyst. The minimum S/C at a given operation temperature and a given biogas composition can be determined by the C–H–O ternary diagram [24].

2.3.2. Post-burner

The exhaust from the SOFC anode containing unreacted CH_4, CO and H_2 is assumed to be fully combusted in the burner through the following reactions,

$$CH_4 + 2O_2 \leftrightarrow CO_2 + 2H_2O \tag{8}$$

$$2CO + O_2 \leftrightarrow 2CO_2 \tag{9}$$

$$2H_2 + O_2 \leftrightarrow 2H_2O \tag{10}$$

The outlet species compositions and outlet temperature of the burner are calculated by the overall mass and energy balance equations.

2.3.3. Further components

The heat exchangers are modeled by the ϵ-NTU method while the air blower is modeled by the isentropic efficiency model, as described in Ref. [42,43]. The other components of the system, such as the mixer and pipes are modeled by the overall mass and energy balance. The BOP models were written in gPROMS language and configured with graphic specifications [44].

2.4. System evaluation parameters

Some parameters are defined to evaluate the system and stack performance. The fuel utilization of the SOFC stack is defined as the ratio between the fuels utilized by electrochemical reactions and input available fuels, which is calculated by

$$U_{f,stack} = \frac{IA}{8F\dot{n}_{a,CH_4,in} + 2F\dot{n}_{a,H_2,in} + 2F\dot{n}_{a,CO,in}} \tag{11}$$

where I is the current density, A is the total active area of the stack, F is the Faraday constant, and $\dot{n}_{a,i,in}$ is the molar flow rate of the anode inlet gas species i. The system electrical efficiency is defined as the ratio between the net power produced and the total chemical energy of the inlet biogas supplied,

$$\eta_{elec,sys} = \frac{P_{SOFC,\,AC} - P_{Blower}}{\dot{m}_{biogas} LHV_{biogas}} \tag{12}$$

where P_{Blower} is the power consumed by the air blower, $\dot{m}_{biogas}$ is the mass flow rate of the inlet biogas, LHV_{biogas} is the lower heating value of the biogas, and $P_{SOFC,AC}$ is the AC power produced by the SOFC and can be calculated by

$$P_{SOFC,\,AC} = P_{SOFC,\,DC} \times \eta_{DC-AC} \tag{13}$$

where η_{DC-AC} is the efficiency of the DC-AC inverter. The system CHP efficiency is defined as the ratio of the net AC power and heat produced by the system and the total chemical energy of the inlet biogas,

$$\eta_{CHP,sys} = \frac{P_{SOFC,\,AC} - P_{Blower} + Q_{heat}}{\dot{m}_{biogas} LHV_{biogas}} \tag{14}$$

where Q_{heat} is the heat recovered by the boiler.

3. Results and discussion

3.1. Base case performance

The SOFC CHP system proposed in this study is designed for hybrid power generation with an AC power output of around 180 kW, which is similar to that of the DEMOSOFC project [45]. The biogas composition is set as the gas composition from WWTPs [24] after clean-up processes. The biogas flow rate is set to ensure a fuel utilization of the SOFC stack around 75%, which falls into a

reasonable range of 60%–80% typically obtained in SOFC systems [34]. Besides, the inlet biogas flow rate is around three times of that in Ref. [33] (20.1 kg h^{-1}) where the AC power output is 60 kW, which further leads credence to the choice of this parameter setting. The base-case operation voltage is set as 0.8 V, which is commonly used as the nominal operating condition in commercial stacks [46]. The operation temperature of the reformer and the inlet air/fuel temperature are set as 973.15 K [24,46]. The S/C ratio of the pre-reformer is set as 0.8, which is higher than the minimum S/C ratio of 0.6 at 973.15 K calculated by the equilibrium C–H–O ternary diagram for the biogas in this system to avoid carbon deposition [24]. The F/A ratio is defined as the ratio between the mass flow rate of the biogas to that of the compressed air. The F/A ratio is set as 0.033 so that the excess air ratio is around 6, which matches the range of 0.36–14 recommended in literature [47]. The system operation conditions at base case are summarized in Table 1.

The base case system performance is evaluated at the above operation conditions and the results are summarized in Table 2. The system produces 180.4 kW AC power along with 95.6 kW heat with $\eta_{elec,sys}$ of 55.4% and $\eta_{CHP,sys}$ of 84.8%. The simulated system performance is further compared with results from recent literatures on biogas-fed SOFC systems, as shown in Table 3. The calculated $\eta_{elec,sys}$ in the current study is not only similar to the simulation results [33,34], but also similar to the experimental data of from DEMOSOFC project [45]. The comparison between the results from the present simulation with those from recent modeling and experimental studies shows that the current model offers reasonable and reliable predictions for biogas-fed SOFC systems.

Except for the general system performance, the current hierarchical system modeling approach allows the acquisition of detailed stack information. Fig. 2 shows the mole fraction distributions of main anode species along the fuel channel and the anode thickness of the repeating unit at the stack center. The reforming products entering SOFC anode channel contains of 51.3% H_2, 22.0% CO, 9.6% CO_2, 13.2% H_2O, 3.3% CH_4 and trace amount of N_2. The mole fraction of H_2 decreases while the mole fraction of H_2O increases along the fuel channel due to the electrochemical oxidation of H_2. For the mole fractions of CO and CO_2, there's a slight increase in x_{CO} and a slight decrease in x_{CO_2} in the first 3 mm of the fuel channel, which is due to the reverse water gas shift (RWGS) reaction. Additionally, the steam reforming reaction of CH_4 leads to a decrease of x_{CH_4} along the fuel channel. As shown in the radial species distributions along the anode thickness direction, the RWGS reaction dominates within the anode in the region spanning less than 100 μm from the electrode-channel interface while the gas diffusion due to the electrochemical reactions at the electrode-electrolyte interface dominates the rest portion of the anode at the fuel cell inlet (z = 1.92 mm). However, at the middle of the fuel cell (z = 47.9 mm), the electrochemical oxidation of H_2 and CO dominates the entire anode domain.

Table 1
Base case operation conditions.

Parameter	Value	Reference
Biogas flow rate (kg h^{-1})	63.5	Estimated
Biogas composition	CH_4 = 61%	[24]
	CO_2 = 37.4%	[24]
	N_2 = 1.6%	Estimated
S/C ratio	0.8	Estimated
Pre-reformer temperature (K)	973.15	[46]
Stack inlet air temperature (K)	973.15	[24]
Air blower isentropic efficiency	85%	[48]
Inlet cold water temperature (K)	313.15	[49]
Outlet hot water temperature (K)	363.15	[49]
DC-AC Inverter efficiency	96%	[34]
F/A ratio	0.033	Estimated
E_{cell} (V)	0.8	[46]

Table 2
Base case system performance.

Parameter	Value
I_{avg} (A cm^{-2})	0.44
T_{avg} (K)	1120
$P_{SOFC,\ AC}$ (kW)	180.4
Q_{heat} (kW)	95.6
$U_{f,stack}$	74.4%
$\eta_{elec,sys}$	55.4%
$\eta_{CHP,sys}$	84.8%

Table 3
Comparison of system electrical efficiency and CHP efficiency between current study and recent studies.

	Current Study	Ref. [34]	Ref. [33]	Ref. [45]
$\eta_{elec,sys}$	55.4%	51.6%	51.12%	> 53%
$\eta_{CHP,sys}$	84.8%	87.5%	–	> 80%

Fig. 3 shows the axial cut-away views of the 3-D temperature distribution of the 50-cell SOFC stack at the base case operation condition. The stack was simulated under co-flow conditions and a heat flux boundary condition considering the convective and radiative heat exchange between the solid stack and the surroundings was set as the boundary condition for the solid temperature. As shown in Fig. 3, there exists a central hot spot within each axial section since the heat released by electrochemical oxidation reactions overwhelms the endothermic steam reforming and RWGS reactions. Moreover, the exothermic effect of the electrochemical reactions also leads to the increase of the stack temperature in the flow direction. From the 3-D stack temperature distribution, the maximum local temperature gradient can be obtained. The temperature gradient is an important parameter for the SOFC stack operation safety since a large temperature gradient may lead to chemical cell degradation and mechanical stack degradation in various ways, such as crack growth in electrolyte, delamination of cell layers, sealing degradation, etc. [50]. For the typical YSZ-based SOFC stack, Aguiar et al. obtained a maximum allowable local thermal gradient of 10 K cm^{-1} by assuming a thermal expansion coefficient of 10^{-5} K^{-1} and a maximum safe strain of 0.1% [51] while Amiri et al. proposed a target of maximum temperature gradient at 15 K cm^{-1} [52]. In this study, ∇T_{max} is found to be 12.1 K cm^{-1} at the base case operation condition, which is higher than that proposed by Aguiar et al. but within the limit of the criterion proposed by Amiri et al. In the following sections, the effects of the system operation conditions on the general system performance and detailed stack performance are further investigated.

3.2. Effect of S/C ratio on system and stack performance

The S/C ratio is a key parameter for the biogas hybrid system since a certain amount of steam is needed to prevent carbon deposition of the pre-reformer. The S/C ratio will determine the compositions of the reformed fuel gases and further influence the stack and system performance. In this section, the S/C ratio is changed by varying the inlet steam flow rate while keeping the other parameters fixed. The system and stack performances are evaluated at S/C ratios of 0.6, 0.8, 1.0 and 1.2 respectively.

Fig. 4 (a) shows the effect of S/C ratio on the mole fractions of the pre-reforming products. As the S/C ratio increases from 0.6 to 1.2, the conversion of methane in the pre-reformer is raised, leading to

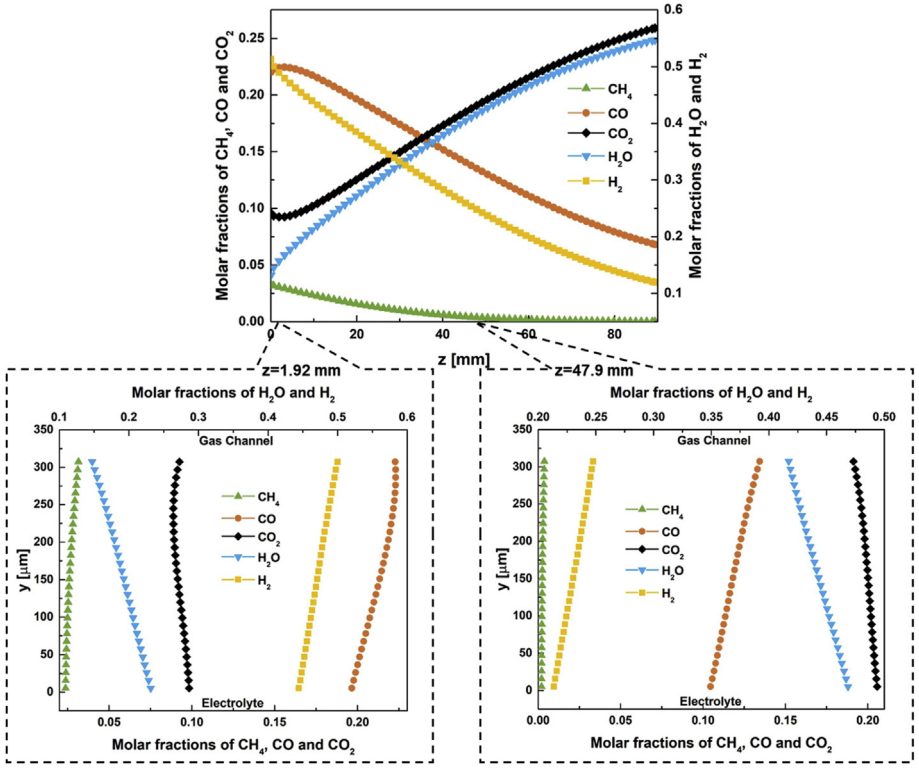

Fig. 2. Mole fractions of chemically reactive anode species as a function of the fuel channel axial position z and the anode radial position y for the repeating unit at the center of the 50-cell stack.

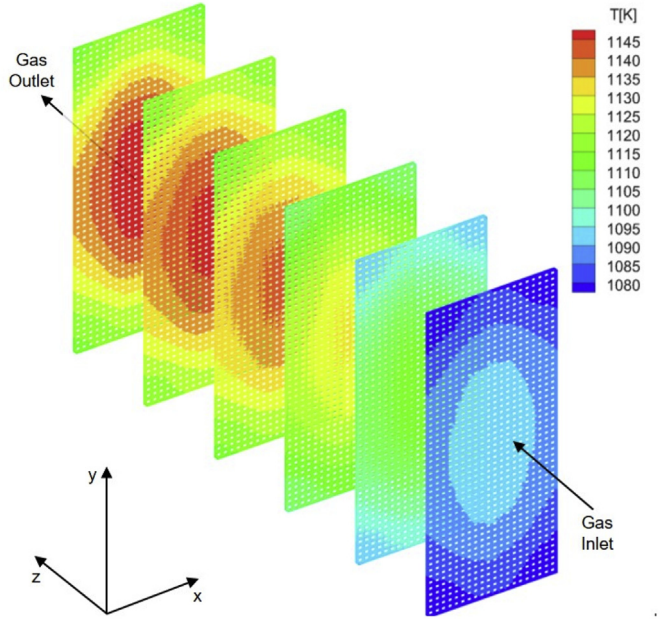

Fig. 3. Temperature distribution of the 50-cell co-flow SOFC stack at the base case operation condition.

a decrease of CH_4 mole fraction. The increasing amount of water also promotes the WGS reaction, thereby consuming CO and producing CO_2. In total, the anode inlet gas contains more oxidative products (CO_2 and H_2O) when increasing the S/C ratio from 0.6 to 1.2.

The SOFC stack temperature is a combined result of the joule heating due to irreversible losses, the reversible heat released by the electrochemical reactions, the heat released/consumed by the thermochemistry on Ni surface and the convective heat exchange between the stack and the inlet gases. Since the anodic gas atmosphere becomes more oxidative at a higher S/C ratio, the joule heating and heat released by the electrochemical reactions both decrease. On the other hand, the decrease of CH_4 mole fraction leads to the decrease of the heat consumption by internal reforming. The above factors result in a slight increase of average stack temperature from 1111 K to 1134 K when the S/C ratio increases from 0.6 to 1.2, as shown in Fig. 4 (b). The maximum stack temperature increases from 1135 K to 1155 K while the minimum stack temperature increases from 1069 K to 1089 K. The corresponding temperature gradient also increases slightly from 11.4 K cm^{-1} to 13.0 K cm^{-1}.

Fig. 4 (c) shows the AC power output and the heat produced by the biogas-fed system at various S/C ratios. The AC power output of the SOFC decreases from 181 kW to 177 kW with the S/C ratio changing from 0.6 to 1.2. However, the heat recovered from the boiler increases from 95.4 kW to 98.7 kW due to an increased outlet temperature of the SOFC stack. The decrease of the AC power output further leads to a decrease of the system electrical efficiency from 55.8% to 54.5%, as shown in Fig. 4 (d). The system CHP efficiency decreases slightly from 85.1% to 84.9% since the evaporator and the pre-reformer consume more heat when the S/C ratio increases. The simulation results thus indicate that the S/C ratio should be set near the minimum S/C ratio to ensure a relatively high system efficiency and low temperature gradient.

3.3. Effect of biogas composition on system and stack performance

In practice, the composition of biogas can vary depending on the properties of the feedstock and the production processes. As

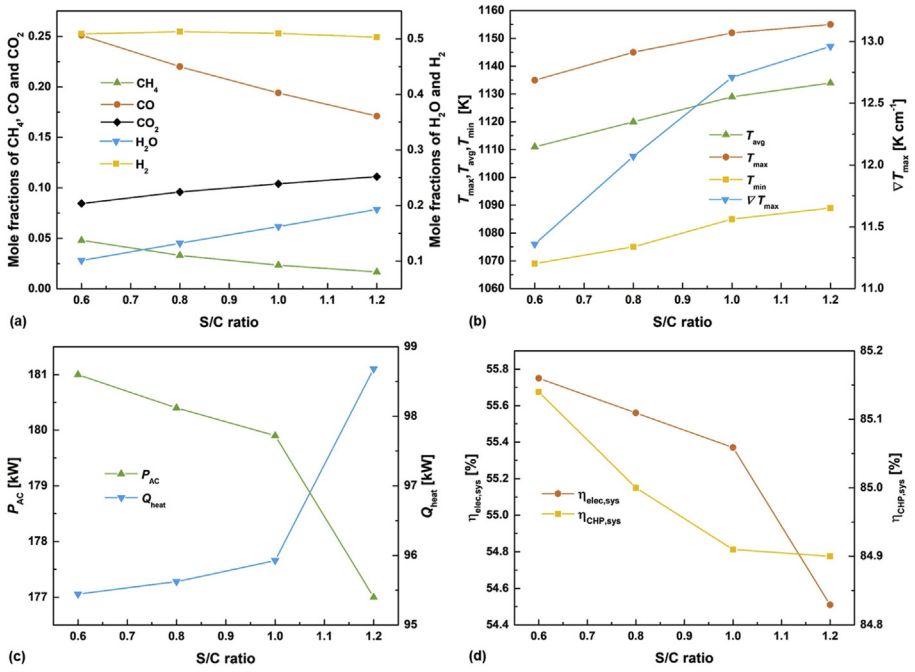

Fig. 4. Effect of S/C ratio on (a) mole fractions of the pre-reforming product (b) maximum, average, minimum temperature and temperature gradient of the stack (c) AC power and heat output of the system (d) electrical and CHP system efficiencies.

mentioned in the introduction, the mole fraction of CH_4 in biogas may vary from 50% to 70% while the mole fraction of CO_2 may vary from 30% to 50%. The biogas composition will influence the composition of the SOFC anode feed gases, further affecting the performance of the SOFC stack and the whole energy system. Thus, it is meaningful to evaluate the stack and system performance when feeding biogases having different compositions.

In this section, the effect of biogas composition on stack and system performance is studied by changing the mole fractions of CH_4 and CO_2 while keeping the other parameters fixed. Three typical biogas compositions are considered with CH_4 mole fractions of 50%, 60%, 70% and the CO_2 mole fractions of 50%, 40%, 30%, respectively. As the mole fraction of CH_4 fed to the reformer increases from 50% to 70%, x_{H2} and x_{CO}, which both enter the stack as fuels, increase from 45.4% to 54.5% and from 20.1% to 23.0% respectively, as shown in Table 4. However, since the inlet flow rate of the water in the pre-reformer keeps unchanged, more CH_4 is unreformed, and thus, the mole fraction of the remaining CH_4 increases from 1.5% to 5.6%.

Carbon deposition might occur at the SOFC anode when feeding the cells with carbonaceous fuels such as biogas. The detailed modeling of the chemical reactions on the electrode level enables the simulation of spatially resolved carbon coverage for various biogas compositions. The surface carbon modeled is a precursor to carbon deposition found in experiments and can act as a prediction of the carbon deposition trend [53]. As shown in Fig. 5, when the mole fraction of methane in biogas increases, the increase of CH_4 and CO and the decrease of H_2O in anode inlet gases favor the tendency of carbon deposition and thereby enhance the carbon coverage. When comparing the carbon coverage at different positions along the fuel channel, it can be found that the carbon coverage decreases by more than one order of magnitude. The average carbon coverages for various biogas compositions are in the range of 1.8–6.7 $\times$ 10^{-6} at the fuel cell inlet (Fig. 5(a)) while those at the middle of the fuel cell are in the range of 0.7–2.2 $\times$ 10^{-7} (Fig. 5(b)). The reason is that the mole fraction of H_2O increases along the axial direction by the production of electrochemical reactions, which counteracts the carbon deposition by the following reaction:

$$C + H_2O \leftrightarrow CO + H_2 \quad (15)$$

As stated by Schluckner et al. [53], the carbon coverage above the magnitude of 10^{-5} may represent an anode exposed to severe carbon deposits while the carbon coverage below the magnitude of 5 $\times$ 10^{-10} may represent an anode free from carbon deposits. The predicted carbon coverages in this study indicate that the SOFC stack faces the risk of carbon deposition for all the biogas compositions considered although an external pre-reformer is applied in the system.

Table 5 shows the effect of biogas composition on both the stack and the system performance. The increase of useful fuels (H_2 and CO) at higher CH_4 mole fractions leads to an increase of average current density from 0.34 to 0.52 A cm^{-2} and an increase of stack AC power output from 140.3 to 212.3 kW. The system electrical efficiency decreases from 59.3% to 52.1% since the fuel utilization of the SOFC stack decreases from 80.3% to 70.6%. However, the heat recovered from the boiler increases from 50.7 kW to 136.6 kW due to both a higher amount of unreacted fuels in the anode exhausts and an increased outlet temperature of the SOFC stack. The increase of the heat recovery offsets the decrease of the electrical efficiency,

Table 4
Effect of the biogas composition on the mole fractions of the pre-reformed gas mixture.

	x_{CH4}:x_{CO2}		
	50%:50%	60%:40%	70%:30%
x_{CH4}	1.5%	3.0%	5.6%
x_{CO}	20.1%	22.0%	23.0%
x_{H2}	45.4%	50.7%	54.5%
x_{CO2}	14.1%	10.3%	7.0%
x_{H2O}	18.9%	14.0%	9.9%

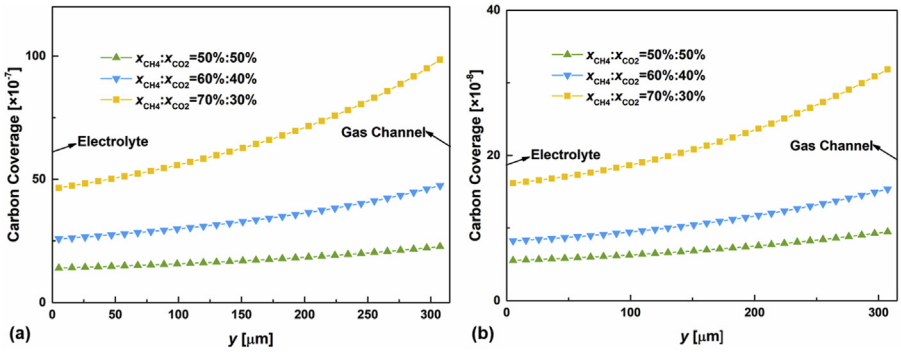

Fig. 5. Carbon coverage as a function of the anode radial position y for the repeating unit at the center of the 50-cell stack at different axial positions (a) z = 1.92 mm (b) z = 47.9 mm.

Table 5
Effect of the biogas composition on the stack and system performance.

	x_{CH4}:x_{CO2}		
	50%:50%	60%:40%	70%:30%
T_{avg} (K)	1097	1117	1131
∇T (K cm^{-1})	10.0	11.9	12.7
I_{avg} (A cm^{-2})	0.34	0.43	0.52
$U_{f.stack}$	80.3%	75.8%	70.6%
P_{AC} (kW)	140.3	175.0	212.3
Q_{heat} (kW)	50.7	90.2	136.6
$\eta_{elec,sys}$	59.3%	55.9%	52.1%
$\eta_{CHP,sys}$	82.4%	84.5%	85.5%

Table 6
Effect of the operation voltage on the stack and system performance.

	Operation Voltage (V)		
	0.78	0.8	0.82
T_{avg} (K)	1147	1120	1106
∇T (K cm^{-1})	13.8	12.1	10.6
I_{avg} (A cm^{-2})	0.49	0.44	0.39
P_{AC} (kW)	197.0	180.4	162.3
Q_{heat} (kW)	72.2	95.6	120.5
$\eta_{elec,sys}$	60.5%	55.6%	49.8%
$\eta_{CHP,sys}$	82.7%	85%	86.9%

which leads to the increase of overall CHP system efficiency from 82.4% to 85.5%.

However, the more significant joule heating and heat released by the electrochemical reactions in the more reducing anode gas atmosphere lead to an increase of the stack average temperature from 1097 K to 1131 K and correspondingly, ∇T changes from 10 K cm^{-1} to 12.7 K cm^{-1}. The increase of the temperature gradient and the higher tendency of carbon deposition at higher inlet CH_4 mole fractions may lead to accelerated stack degradation. The temperature gradient may lead to crack growth and other mechanical degradation [50]. The carbon deposition may block the active sites of the anode, reduce the porosity and cause morphology changes of the anode structure, which further leads to a decrease of electrochemical activity and an increase of gas transport resistance respectively [12]. Besides, if biogas is not properly purified, the impurities in real biogas such as H_2S, HCl and siloxanes may accumulate at the anode/electrolyte interface and lead to a decrease of the electrochemical activity and reversible/irreversible degradation of the cell performance. The interested reader may be referred to some related publications to gain detailed information on degradation mechanisms caused by fuel contaminants in biogas [12,54].

3.4. Effect of operation voltage on system and stack performance

In this section, the effect of the operation voltage of the SOFC on the stack and system performance is analyzed and the results are shown in Table 6. It should be noted that all the other operation parameters except for the operation voltage are kept unchanged. As the operation voltage increases from 0.78 V to 0.82 V, the average current density decreases from 0.49 A cm^{-2} to 0.39 A cm^{-2}. The overheating due to exothermic electrochemical process becomes less severe at the higher operation voltage. Thus, the average stack temperature decreases from 1147 K to 1106 K and ∇T decreases from 13.8 K cm^{-1} to 10.6 K cm^{-1}.

The decrease of average current density further leads to a decrease of P_{AC} from 197.0 kW to 162.3 kW when increasing the operation voltage from 0.78 V to 0.82 V. Since the chemical energy of the inlet biogas kept unchanged, the system electrical efficiency correspondingly decreases from 60.5% to 49.8%. There exist more unreacted fuels in the anode outlet gases at a higher operation voltage. As a result, more chemical energy is converted to heat in the burner and the burner outlet temperature increases from 1239 K to 1311 K. The heat recovered by the boiler increases from 72.2 kW to 120.5 kW. The overall CHP system efficiency increases from 82.7% to 86.9% since the heat recovery gain more than offsets the decreased electrical efficiency. The SOFC lifetime specific energy cost is dependent on not only the investment cost, but also the efficiency, power density and degradation [50]. On one hand, the decrease of temperature gradient at a higher voltage has a positive influence on degradation rates and the SOFC lifetime [55]. However, on the other hand, the lower power output and system electrical efficiency at a higher operation voltage will increase the specific energy cost. Trendewicz et al. concluded that with an electrical efficiency of 51.6% and a CHP efficiency of 87.5%, the SOFC-based system is economically competitive with other CHP systems based on reciprocating engines, micro turbines and MCFCs [34]. While, the results of Giarola et al. showed that the electrical efficiency of the SOFC-based system should reach around 60% to have the comparable costs to the best conventional alternatives [32]. Based on the current research, a detailed techno-economic analysis and a multi-objective optimization could be carried out to meet the conflicting targets of the temperature gradient and electrical efficiency.

4. Conclusions

A multi-scale model was developed in this study for the assessment of a biogas-fed SOFC hybrid CHP system. The system model successfully integrated a hierarchical 3-D SOFC stack model with 0-D models of BOP components such as a pre-reformer, a post-

burner, an evaporator, a mixer, heat exchangers, etc. The system model considered detailed modeling from electrode level to stack and system level, which yield new insights into the efficient and reliable operation of biogas SOFC systems. The hierarchical modeling approach enabled the simultaneous investigations of both the overall system performance and the spatially resolved internal SOFC stack state down to the electrode level. The system electrical efficiency and CHP efficiency reached 55.6% and 85%, respectively, at the base case operation conditions. The effects of the S/C ratio of the pre-reformer, the biogas composition and the operation voltage of the SOFC stack on the system and stack performance were analyzed. The increase of the S/C ratio leads to a decrease of both system electrical and CHP efficiency and an increase of the stack temperature gradient. Thus, the S/C ratio should be set near the minimum S/C ratio to ensure a relatively high efficiency and low temperature gradient. The increase of CH_4 mole fraction in biogas leads to a decreased system electrical efficiency and an increased CHP efficiency. The electrical efficiency remains higher than 50% and the CHP system efficiency remains higher than 80% for all the typical compositions considered, which demonstrates the feasibility of the system structure at various biogas compositions. However, the stack durability may decrease with increasing CH_4 in biogas due to the increase of both the temperature gradient and the carbon coverage on the electrodes. The increase of operation voltage leads to the decrease of the system electrical efficiency and the stack temperature gradient but an increase of the system CHP efficiency.

CRediT authorship contribution statement

Yuqing Wang: Conceptualization, Methodology, Software, Investigation, Writing - original draft, Funding acquisition. **Lukas Wehrle:** Software, Validation, Writing - review & editing. **Aayan Banerjee:** Software, Writing - review & editing. **Yixiang Shi:** Software. **Olaf Deutschmann:** Supervision, Writing - review & editing.

Declaration of competing interest

The authors declare that they have no known competing financial interests or personal relationships that could have appeared to influence the work reported in this paper.

Acknowledgments

We thank the Steinbeis GmbH & Co KG für Technologietransfer (STZ 240 Reaktive Strömungen) for a cost free academic license of DETCHEM™. We would also like to thank our colleague Dr. Steffen Tischer from Karlsruhe Institute of Technology for his help in generating the axial cut away views of the 3-D stack temperature profiles. The research is supported by Beijing National Science Foundation, China, 3194058, National Natural Science Foundation of China, China, 51806017 and the Beijing Institute of Technology Research Fund Program for Young Scholars. The funding provided by Alexander von Humboldt Foundation for Y. Wang for a half-year research stay at KIT is highly appreciated.

Nomenclature

Abbreviation

0-D	zero-dimensional
1-D	one-dimensional
3-D	three-dimensional
AC	alternating current
BOP	balance of plant
CHP	combined heat and power
DC	direct current
F/A	fuel/air
GT	gas turbine
I/O	input/output
LHV	lower heating value
MGT	micro gas turbine
S/C	steam/carbon
SOFC	solid oxide fuel cell
SR	steam reforming
WGS	water gas shift
WWTPs	wastewater treatment plants

English letters

E	operation voltage (V)
F	Faraday constant (=96,485 C mol^{-1})
h	mass enthalpy (J kg^{-1})
I	current density (A cm^{-2})
K_{eq}	equilibrium constant
$\dot{m}$	mass flow rate (kg s^{-1})
$\dot{n}$	molar flow rate (mol s^{-1})
p	pressure (Pa)
P	power (W)
Q	heat (W)
T	temperature (K)
U_f	fuel utilization
x	mole fraction
y	mass fraction

Greek letters

η	efficiency

Subscripts and superscripts

a	anode
avg	average
elec	electrical
H	hot
in	inlet parameter
out	outlet parameter
sys	system

References

[1] J. Xuan, M.K. Leung, D.Y. Leung, M. Ni, A review of biomass-derived fuel processors for fuel cell systems, Renew. Sustain. Energy Rev. 13 (2009) 1301–1313.
[2] X. Ding, X. Lv, Y. Weng, Coupling effect of operating parameters on performance of a biogas-fueled solid oxide fuel cell/gas turbine hybrid system, Appl. Energy 254 (2019), 113675.
[3] A. Hawkes, I. Staffell, D. Brett, N. Brandon, Fuel cells for micro-combined heat and power generation, Energy Environ. Sci. 2 (2009) 729–744.
[4] H. Zhang, J. Wang, F. Wang, J. Zhao, H. Miao, J. Yuan, Performance assessment of an advanced triple-cycle system based upon solid oxide fuel cells, vacuum thermionic generators and absorption refrigerators, Energy Convers. Manag. 193 (2019) 64–73.
[5] H. Zhang, W. Kong, F. Dong, H. Xu, B. Chen, M. Ni, Application of cascading thermoelectric generator and cooler for waste heat recovery from solid oxide fuel cells, Energy Convers. Manag. 148 (2017) 1382–1390.
[6] S.A. Saadabadi, A.T. Thattai, L. Fan, R.E. Lindeboom, H. Spanjers, P.V. Aravind, Solid oxide fuel cells fuelled with biogas: potential and constraints, Renew. Energy 134 (2019) 194–214.
[7] Y. Shiratori, T. Oshima, K. Sasaki, Feasibility of direct-biogas SOFC, Int. J. Hydrogen Energy 33 (2008) 6316–6321.
[8] Y. Shiratori, T. Ijichi, T. Oshima, K. Sasaki, Internal reforming SOFC running on biogas, Int. J. Hydrogen Energy 35 (2010) 7905–7912.
[9] H. Madi, S. Diethelm, S. Poitel, C. Ludwig, J. Van Herle, Damage of siloxanes on Ni-YSZ anode supported SOFC operated on hydrogen and bio-syngas, Fuel Cell. 15 (2015) 718–727.
[10] D. Papurello, A. Lanzini, SOFC single cells fed by biogas: experimental tests with trace contaminants, Waste Manag. 72 (2018) 306–312.
[11] H. Madi, S. Diethelm, C. Ludwig, J. Van Herle, Organic-sulfur poisoning of solid

oxide fuel cell operated on bio-syngas, Int. J. Hydrogen Energy 41 (2016) 12231–12241.
[12] A. Lanzini, D. Ferrero, D. Papurello, M. Santarelli, Reporting degradation from different fuel contaminants in Ni-anode SOFCs, Fuel Cell. 17 (2017) 423–433.
[13] A. Fuerte, R.X. Valenzuela, M.J. Escudero, L. Daza, Study of a SOFC with a bimetallic Cu-Co-ceria anode directly fuelled with simulated biogas mixtures, Int. J. Hydrogen Energy 39 (2014) 4060–4066.
[14] Y. Shiratori, M. Sakamoto, Performance improvement of direct internal reforming solid oxide fuel cell fuelled by H_2S-contaminated biogas with paper-structured catalyst technology, J. Power Sources 332 (2016) 170–179.
[15] D. Papurello, A. Lanzini, P. Leone, M. Santarelli, S. Silvestri, Biogas from the organic fraction of municipal solid waste: dealing with contaminants for a solid oxide fuel cell energy generator, Waste Manag. 34 (2014) 2047–2056.
[16] D. Papurello, A. Lanzini, L. Tognana, S. Silvestri, M. Santarelli, Waste to energy: exploitation of biogas from organic waste in a 500 Wel solid oxide fuel cell (SOFC) stack, Energy 85 (2015) 145–158.
[17] M. Santarelli, M. Gandiglio, M. Acri, T. Hakala, M. Rautanen, A. Hawkes, Results from industrial size biogas-fed SOFC plant (DEMOSOFC Project), ECS Trans. 91 (2019) 107–116.
[18] G.N. Prodromidis, F.A. Coutelieris, Thermodynamic analysis of biogas fed solid oxide fuel cell power plants, Renew. Energy 108 (2017) 1–10.
[19] P. Boldrin, E. Ruiztrejo, J. Mermelstein, J.M. Menendez, T.R. Reina, N.P. Brandon, Strategies for carbon and sulfur tolerant solid oxide fuel cell materials, incorporating lessons from heterogeneous catalysis, Chem. Rev. 116 (2016) 13633–13684.
[20] W. Wang, C. Su, Y. Wu, R. Ran, Z. Shao, Progress in solid oxide fuel cells with nickel-based anodes operating on methane and related fuels, Chem. Rev. 113 (2013) 8104–8151.
[21] H. Xu, B. Chen, P. Tan, W. Cai, W. He, D. Farrusseng, M. Ni, Modeling of all porous solid oxide fuel cells, Appl. Energy 219 (2018) 105–113.
[22] R. Cozzolino, L. Lombardi, L. Tribioli, Use of biogas from biowaste in a solid oxide fuel cell stack: application to an off-grid power plant, Renew. Energy 111 (2017) 781–791.
[23] B. Tjaden, M. Gandiglio, A. Lanzini, M. Santarelli, M. Jarvinen, Small-scale biogas-SOFC plant: technical analysis and assessment of different fuel reforming options, Energy Fuels 28 (2014) 4216–4232.
[24] S. Farhad, Y. Yoo, F. Hamdullahpur, Effects of fuel processing methods on industrial scale biogas-fuelled solid oxide fuel cell system for operating in wastewater treatment plants, J. Power Sources 195 (2010) 1446–1453.
[25] F. Manenti, R. Pelosato, P. Vallevi, A.R. Leon-Garzon, G. Dotelli, A. Vita, A.S. Aricò, Biogas-fed solid oxide fuel cell (SOFC) coupled to tri-reforming process: modelling and simulation, Int. J. Hydrogen Energy 40 (2015) 14640–14650.
[26] G. D'Andrea, M. Gandiglio, A. Lanzini, M. Santarelli, Dynamic model with experimental validation of a biogas-fed SOFC plant, Energy Convers. Manag. 135 (2017) 21–34.
[27] S. Wongchanapai, H. Iwai, M. Saito, H. Yoshida, Performance evaluation of a direct-biogas solid oxide fuel cell-micro gas turbine (SOFC-MGT) hybrid combined heat and power (CHP) system, J. Power Sources 223 (2013) 9–17.
[28] X. Ding, X. Lv, Y. Weng, Effect of operating parameters on performance and safety evaluation of a biogas-fueled SOFC/GT hybrid system, Energy Procedia 158 (2019) 1842–1849.
[29] A.S. Mehr, M. MosayebNezhad, A. Lanzini, M. Yari, S.M.S. Mahmoudi, M. Santarelli, Thermodynamic assessment of a novel SOFC based CCHP system in a wastewater treatment plant, Energy 150 (2018) 299–309.
[30] K. Hauptmeier, M. Penkuhn, G. Tsatsaronis, Economic assessment of a solid oxide fuel cell system for biogas utilization in sewage plants, Energy 117 (2016) 361–368.
[31] O.J. Shariatzadeh, A.H. Refahi, M. Rahmani, S.S. Abolhassani, Economic optimisation and thermodynamic modelling of SOFC tri-generation system fed by biogas, Energy Convers. Manag. 105 (2015) 772–781.
[32] S. Giarola, O. Forte, A. Lanzini, M. Gandiglio, M. Santarelli, A. Hawkes, Techno-economic assessment of biogas-fed solid oxide fuel cell combined heat and power system at industrial scale, Appl. Energy 211 (2018) 689–704.
[33] M. MosayebNezhad, A.S. Mehr, M. Gandiglio, A. Lanzini, M. Santarelli, Techno-economic assessment of biogas-fed CHP hybrid systems in a real wastewater treatment plant, Appl. Therm. Eng. 129 (2018) 1263–1280.
[34] A.A. Trendewicz, R.J. Braun, Techno-economic analysis of solid oxide fuel cell-based combined heat and power systems for biogas utilization at wastewater treatment facilities, J. Power Sources 233 (2013) 380–393.
[35] O. Deutschmann, S. Tischer, S. Kleditzsch, V. Janardhanan, C. Correa, D. Chatterjee, N. Mladenov, H.D. Minh, H. Karadeniz, M. Hettel, V. Menon, A. Banerjee, H. Gossler, DETCHEM Software package, 2.8, Karlsruhe, www.detchem.com, 2019.
[36] V. Menon, V.M. Janardhanan, S. Tischer, O. Deutschmann, A novel approach to model the transient behavior of solid-oxide fuel cell stacks, J. Power Sources 214 (2012) 227–238.
[37] A. Banerjee, Y. Wang, J. Diercks, O. Deutschmann, Hierarchical modeling of solid oxide cells and stacks producing syngas via H_2O/CO_2 co-electrolysis for industrial applications, Appl. Energy 230 (2018) 996–1013.
[38] L. Maier, B. Schädel, K.H. Delgado, S. Tischer, O. Deutschmann, Steam reforming of methane over nickel: development of a multi-step surface reaction mechanism, Top. Catal. 54 (2011) 845.
[39] S.D. Ebbesen, C. Graves, M. Mogensen, Production of synthetic fuels by co-electrolysis of steam and carbon dioxide, Int. J. Green Energy 6 (2009) 646–660.
[40] L. Wehrle, Y. Wang, A. Banerjee, N. Brandon, O. Deutschmann, Dynamic modeling of reversible solid oxide cells, Chem. Ing. Tech. 91 (2019) 833–842.
[41] Q. Fu, J. Dailly, A. Brisse, M. Zahid, High-temperature CO_2 and H_2O electrolysis with an electrolyte-supported solid oxide cell, ECS Trans. 35 (2011) 2949–2956.
[42] Y. Wang, A. Banerjee, L. Wehrle, Y. Shi, N. Brandon, O. Deutschmann, Performance analysis of a reversible solid oxide cell system based on multi-scale hierarchical solid oxide cell modelling, Energy Convers. Manag. 196 (2019) 484–496.
[43] C. Bao, N. Cai, E. Croiset, A multi-level simulation platform of natural gas internal reforming solid oxide fuel cell–gas turbine hybrid generation system–Part II. Balancing units model library and system simulation, J. Power Sources 196 (2011) 8424–8434.
[44] C. Bao, Y. Shi, C. Li, N. Cai, Q. Su, Multi-level simulation platform of SOFC-GT hybrid generation system, Int. J. Hydrogen Energy 35 (2010) 2894–2899.
[45] M. Gandiglio, A. Lanzini, M. Santarelli, M. Acri, T. Hakala, M. Rautanen, Results from an industrial size biogas-fed SOFC plant (the DEMOSOFC project), Int. J. Hydrogen Energy 45 (2020) 5449–5464.
[46] V. Chiodo, A. Galvagno, A. Lanzini, D. Papurello, F. Urbani, M. Santarelli, S. Freni, Biogas reforming process investigation for SOFC application, Energy Convers. Manag. 98 (2015) 252–258.
[47] P. Aguiar, C.S. Adjiman, N.P. Brandon, Anode-supported intermediate-temperature direct internal reforming solid oxide fuel cell: II. Model-based dynamic performance and control, J. Power Sources 147 (2005) 136–147.
[48] P. Mottaghizadeh, S. Santhanam, M.P. Heddrich, K.A. Friedrich, F. Rinaldi, Process modeling of a reversible solid oxide cell (r-SOC) energy storage system utilizing commercially available SOC reactor, Energy Convers. Manag. 142 (2017) 477–493.
[49] S. Farhad, F. Hamdullahpur, Y. Yoo, Performance evaluation of different configurations of biogas-fuelled SOFC micro-CHP systems for residential applications, Int. J. Hydrogen Energy 35 (2010) 3758–3768.
[50] M. Dillig, Thermal management of solid oxide cell systems with integrated planar heat pipes [ph.D.], erlangen: friedrich-alexander-universität erlangen-nürnberg (FAU), 2016.
[51] P. Aguiar, C.S. Adjiman, N.P. Brandon, Anode-supported intermediate-temperature direct internal reforming solid oxide fuel cell: II. Model-based dynamic performance and control, J. Power Sources 147 (2005) 136–147.
[52] A. Amiri, S. Tang, P. Vijay, M.O. Tadé, Planar solid oxide fuel cell modeling and optimization targeting the stack's temperature gradient Minimization, Ind. Eng. Chem. Res. 55 (2016) 7446–7455.
[53] C. Schluckner, V. Subotic, V. Lawlor, C. Hochenauer, CFD-simulation of effective carbon gasification strategies from high temperature SOFC Ni-YSZ cermet anodes, Int. J. Hydrogen Energy 42 (2017) 4434–4448.
[54] D. Papurello, A. Lanzini, S.L. Fiorilli, F. Smeacetto, R. Singh, M. Santarelli, Sulfur poisoning in Ni-anode solid oxide fuel cells (SOFCs): deactivation in single cells and a stack, Chem. Eng. J. 283 (2016) 1224–1233.
[55] S. Tang, A. Amiri, M.O. Tadé, System level exergy assessment of strategies deployed for solid oxide fuel cell stack temperature regulation and thermal gradient reduction, Ind. Eng. Chem. Res. 58 (2019) 2258–2267.